Light-Emitting Polymer Single Nanofibers *via* Waveguiding Excitation

Fuxing Gu, Huakang Yu, Pan Wang, Zongyin Yang, and Limin Tong*

Department of Optical Engineering, State Key Laboratory of Modern Optical Instrumentation, Zhejiang University, Hangzhou 310027, China

ABSTRACT We report a general approach to light-emitting polymer nanofibers (PNFs) based on waveguiding excitation. By waveguiding excitation light along the PNFs, we demonstrated that the interaction of light with PNFs is enhanced over 3 orders of magnitude compared with the currently used irradiating excitation. Intriguing advantages such as enhanced excitation efficiency, low excitation power operation down to nW levels, tightly confined excitation with low cross talk, and high photostability of the light-emitting PNFs are obtained. The waveguiding excitation allows incorporation of various fluorescent dyes into PNFs to generate multicolor emitting sources covering the entire visible spectrum. The light-emitting single PNFs *via* waveguiding excitation may find widespread nanophotonic applications in chemical and biological sensors, multicolor emitting sources, and lasers.

*Address correspondence to phytong@zju.edu.cn.

The development of ultracompact nanophotonic integrated system are challenging directions in next-generation all-optical signal processing, in which light-emitting sources are important elements for integration.[1,2] In the past decades, doped glass optical fibers have been widely used as solid hosts for photonic applications such as tunable lasers and amplifiers for optical communication.[3,4] For most widely used rare-earth-doped glass fibers, the concentrations of rare-earth dopants are limited by the concentration quenching, for example, typically lower than 1% for Er^{3+} in silica fibers, resulting in relatively low energy conversion efficiency within a limited length. Therefore, it is difficult to obtain efficient energy conversion in doped glass fibers within a scale comparable to the compactness of a nanophotonic integrated system (*e.g.*, on submm level). Recently, key progresses have been made on polymer single nanowires or nanofibers (PNFs) to yield subwavelength multicolor light sources[5−12] and optically pumped lasers.[13−15] Compared to those of glass fibers, the most attractive prospects of PNFs are as follows: First, the polymer matrix can host functional dopants ranging from metal oxides and fluorescent dyes to enzymes that can be used to tailor the properties of the PNFs with greater versatility. Second, the dopants can be easily doped into the solvated polymer and drawn into PNFs at room temperature with higher doping concentration than that in glass fibers. Also, the mechanical flexibility, perm-selective nature to gas molecules, biocompatibility, easy processing, and low cost of the polymer materials,[16] offers more opportunities for doped PNFs over doped glass fibers in nanophotonic systems. Especially, high-efficient light emission dopants (*e.g.*, fluorescent dyes), which are much more compatible with PNFs, show great potential to realize compact light-emitting sources with feature sizes acceptable in nanophotonic integrated systems.

To date, single-doped PNFs are excited by direct irradiation using focused light with spot size on the micrometer scale (typically from several to tens of micrometers), much larger than the acceptance width of a PNF (tens to hundreds of nanometers). Moreover, because of the relatively weak absorption coefficient of PNFs (α, typically in the range of 10 to a few 10^4 cm^{-1}), the excitation light is not sufficiently harvested when penetrating the thin diameter of a PNF. Therefore, these size incompatibilities often lead to low excitation efficiency, high excitation power consumption (above hundreds of microwatts), large excitation spot size, and cross talk.[5−15]
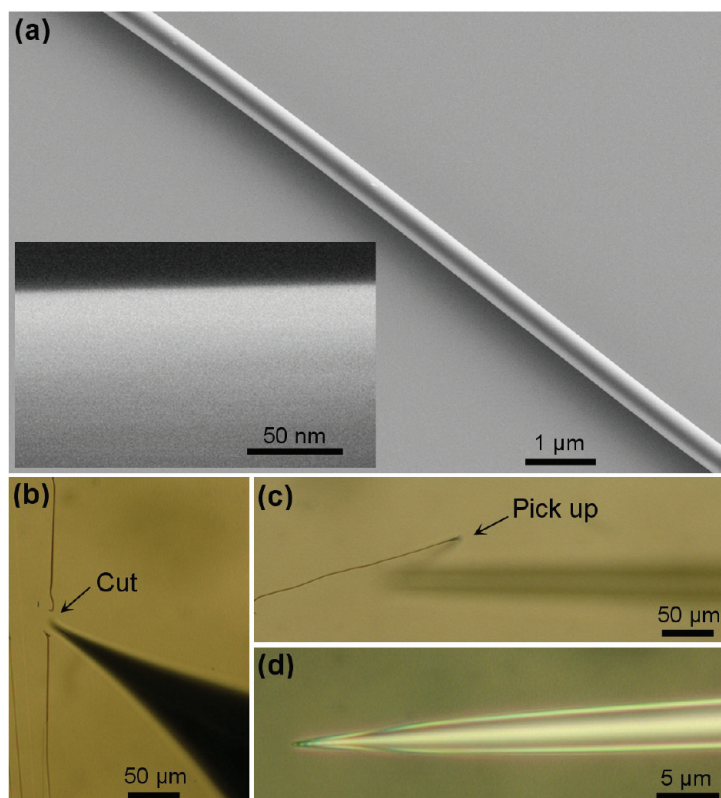
Recently, there is growing attention to a confirmed feature that, in waveguiding single nanowires or nanofibers (NFs), such as semiconductor nanowires,[17−19] the tight confinement of light during its waveguiding along the long length (usually tens to

Figure 1. Characterization and micromanipulation of the dye-doped PNFs. (a) SEM image of a 400-nm-diameter RhB-PS NF. Inset, high-resolution SEM image of the NF. (b) Cutting a NF using a sharp tungsten probe. (c and d) Picking up a NF using a silica fiber taper with a sharp tip size less than 300 nm.

hundreds of micrometers) will enhance the interaction of light with the NFs, which exhibits attractive advantages such as high spatial resolution, enhanced optical sensitivity, and reduced lasing threshold. Here we report a general approach to light-emitting PNFs based on waveguiding excitation. The excitation light is evanescently coupled[20−22] into PNFs from silica fiber tapers and guided along the PNFs, and the PNF−light interaction is enhanced over 3 orders of magnitude compared to the conventional light irradiation scheme. Intriguing advantages such as enhanced excitation efficiency, low excitation power down to nW levels, tightly confined excitation with low cross talk, and high photostability of the light-emitting PNFs are obtained.

We fabricated PNFs by directly drawing from polymer solutions with dissolved fluorescent dyes (see Methods). As-fabricated PNFs have lengths up to several millimeters with diameters selectable from 100 to 800 nm, which is an optimal diameter range for guiding visible and near-infrared light regarding easy handling and efficient in/out coupling. A typical scanning electron microscope (SEM) image of a 310-nm-diameter polystyrene (PS) NF doped with rhodamine B (RhB) is shown in Figure 1a, in which the excellent uniformity and sidewall smoothness is clearly seen. For individual PNFs, the diameter variations ΔD are very small. For example, in a doped PS NF with average diameter of 400 nm, ΔD is about 30 nm over a 1-mm length. The high-

resolution SEM image (inset) shows that there are no obvious defects (*e.g.*, porosity or surface texture) on the surface of the NF. The lengths and diameters of the NFs can be roughly controlled by tuning the viscosity of the solutions.[23] For experimental uses, the NFs are first cut by a sharp tungsten probe *via* micromanipulation (Figure 1b), and then picked up (Figure 1c), transferred, and deposited on a low-index MgF_2 substrate
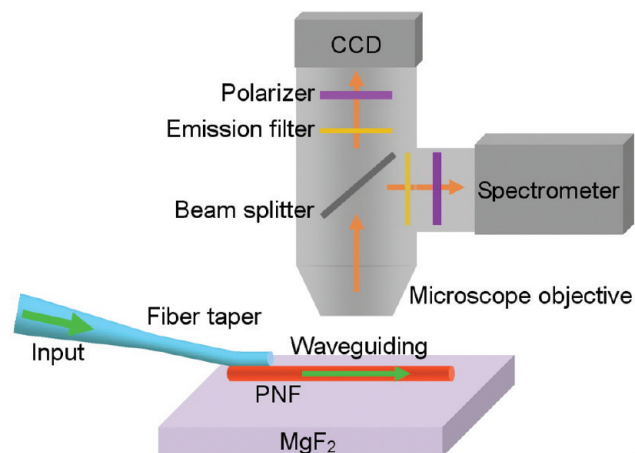
Figure 2. Schematic diagram of an experimental setup for waveguiding excitation of the single PNF supported with a low-index MgF_2 substrate. The excitation light is evanescently launched into the NF, which is precisely controlled by a micromanipulator. The fluorescent emission is picked up using a long working distance objective. Polarizers and emission filters are placed between the samples and the detectors (the spectrometer and the CCD).
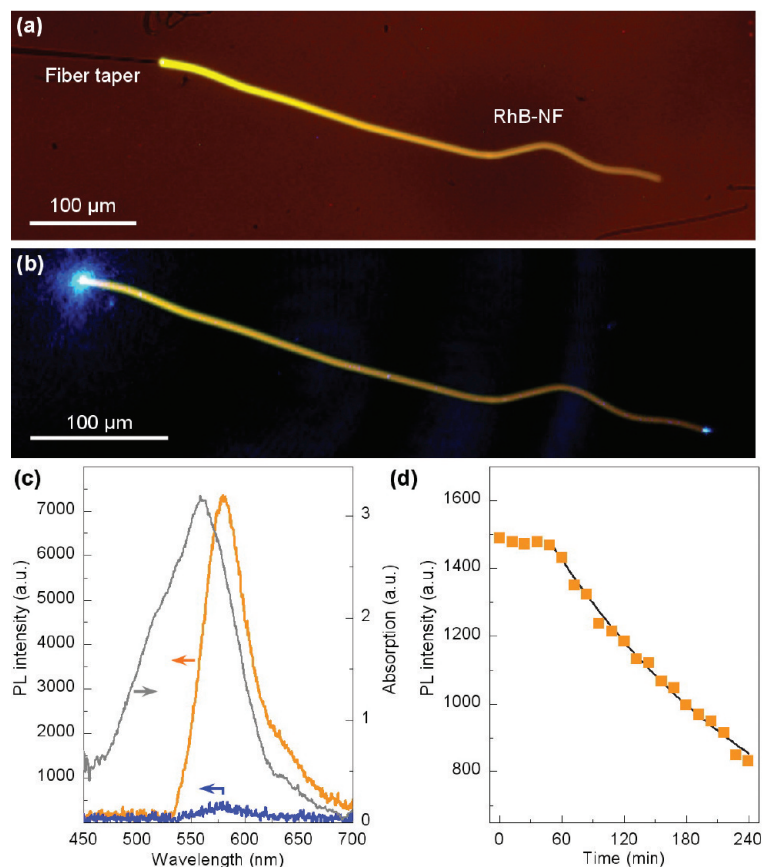
Figure 3. PL microscope images of a 380-nm-diameter 520-μm-length RhB-PS NF excited by 473-nm light from the left side at P_{ex} = 70 nW, taken with (a) and without (b) the long-pass emission filter. (c) PL spectra of the RhB-PS NF under 70-nW waveguiding (orange line) and 3-μW irradiation (blue line) schemes. The absorption spectrum of the NF is also provided (black line). (d) PL intensity of the RhB-PS NF at 579 nm with P_{ex} = 30 nW as a function of time.

(refractive index ≈ 1.39) by a fiber taper with a tip size less than 300 nm fabricated from a standard single-mode silica optical fiber (SMF-28e, Corning), as shown in Figure 1d.

To couple the excitation light efficiently into the PNFs, we employed the evanescent coupling technique due to its high efficiency and high compactness for broadband application.[20−22] In our approach, continuous-wave (cw) light was first lens-coupled into a standard silica fiber and then squeezed into a fiber taper with tip diameter in the range of 300−800 nm. By placing the fiber taper and the NF in parallel and close contact within a few micrometers' overlap as schematically illustrated in Figure 2, optical near-field in the fiber taper and the NF may strongly overlap, resulting in highly efficient coupling (up to 90% in experiments).[24] The close contact between the NF and the fiber taper can be maintained by van der Waals and electrostatic attraction.

Figure 3a shows a photoluminescence (PL) microscope image of a 380-nm-diameter 520-μm-length RhB-PS NF taken with a long-pass emission filter. Upon 473-nm laser (λ_{ex}) launched from the left side with excitation power (P_{ex}) of 70 nW, bright fluorescent emission with a peak (λ_{em}) around 578 nm is generated and guided along the NF. The PL intensity of the RhB-PS

NF decreases exponentially with distance along the NF,[6,7,14,15] attributed to the exponential absorption of the excitation light along the NF by fluorescent dyes obeying the Lambert−Beer law.[25] For reference, Figure 3b shows the PL image taken without the emission filter, in which a small light spot at the output end of the NF and no obvious scattering along the NF are observed, suggesting that the excitation light was efficiently absorbed during its waveguiding excitation. The absorption spectrum of the RhB-PS NF in Figure 3c (black line) exhibits a peak at 560 nm due to the absorption of the doped RhB molecules. The measured absorption coefficient α of the RhB-PS NFs at 473 nm is ∼50 cm^{-1}.

To demonstrate the enhanced excitation efficiency η_{ex} (defined as $\eta_{ex} = P_{em}/P_{ex}$, where P_{em} is the PL emission power of the PNFs) of the waveguiding excitation compared to the irradiation scheme, we show the PL spectrum of the waveguiding RhB-PS NF with P_{ex} = 70 nW in Figure 3c (orange line), in which an obvious PL signal is observed. For comparison, under laser irradiation (spot size, ∼20 μm in diameter), no obvious PL signals were observed until P_{ex} increased as high as ∼3 μW (blue line). Thus the estimated excitation efficiency of the waveguiding scheme is ∼2000 times higher than
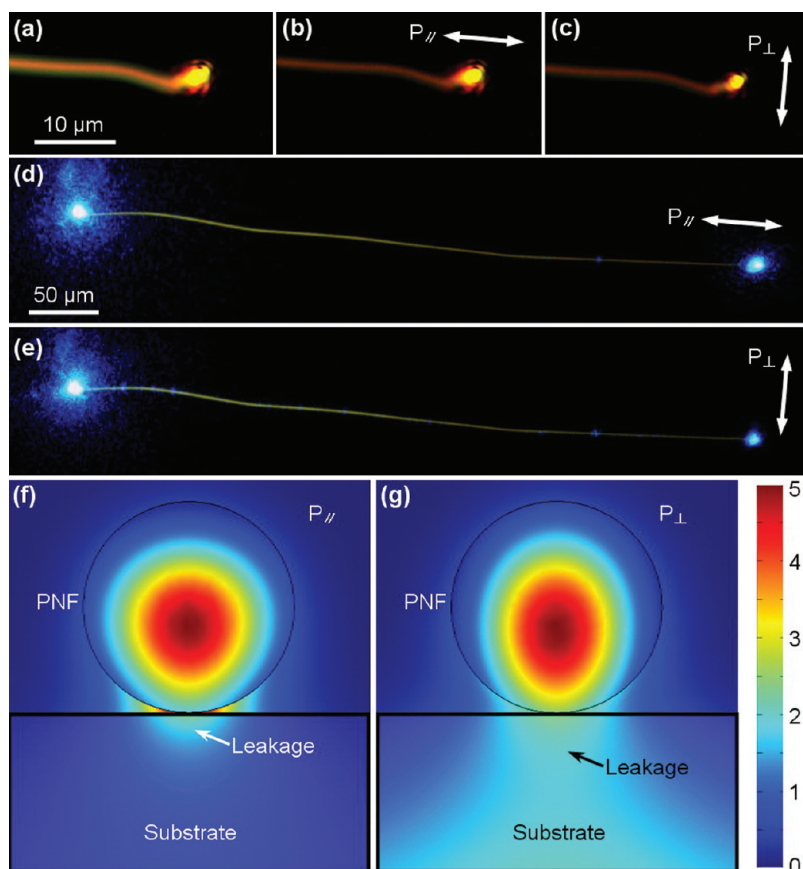
Figure 4. PL microscope images of the output end of a 460-nm-diameter RhB-PS NF taken without (a) and with the polarization parallel (b) and perpendicular (c) to the NF, respectively, at P_{ex} = 80 nW with the long-pass emission filter. (d and e) Microscope images of the polarization behavior of the RhB-PS NF taken at P_{ex} = 80 nW without the long-pass emission filter. (f and g) Power distributions (Poynting vectors) of the guided $P_{\parallel}$ (f) and $P_{\perp}$ (g) modes at the transverse cross plane of the 460-nm-diameter NF.

that of the irradiation scheme with normalized excitation power.

The relationship between P_{em} and P_{ex} can be expressed as[25]

$$P_{em} \propto \xi P_{ex}(1 - 10^{-\alpha L}) \tag{1}$$

where ξ is the effective percentage of P_{ex} accepted by the RhB-PS NFs (includes both absorbed and penetrated light in the NFs), and L is the absorption length. Therefore, the significant enhancement of the excitation efficiency in the waveguiding RhB-PS NFs is attributed to two factors: First, compared with the irradiation scheme that harvests light directly going through the thickness of the NF (L = 380 nm), here light is forced to guide along the length of the NF (L = 520 μm). Second, under the irradiation scheme the ξ in NF is ~2% by comparing the effective area (0.38 μm × 20 μm) with the laser spot area (20 μm in diameter). Here with high efficiency for coupling light from the fiber taper to the NF, the ξ can be as high as over 90% theoretically. Thus according to the relationship 1, a calculated theoretical enhancement ~10000 times of magnitude of the emission power can be obtained. The lower experimental value of ~2000 is mainly due to the additional

optical loss of waveguiding system, suggesting the possibility of further improvement in enhancement.

Also, compared with the irradiation with micrometer-scale light spot, the waveguiding excitation scheme is best adapted for tightly confined excitation with low cross-talk when multiple PNFs are closely located, which are particularly desirable for miniaturization and high-density integration of light-emitting nanodevices.

The enhanced excitation efficiency allows low excitation power operation, which is helpful to decreasing the photobleaching of fluorescent dye in PNFs since the rate of photobleaching closely depends on the light intensity. The PL intensity at λ_{em} = 579 nm of the RhB-PS NF with P_{ex} = 30 nW as a function of time is plotted in Figure 3d, in which obvious photobleaching starts after 50 min obeying an exponential decay. After 3 h of waveguiding excitation, over 50% of the initial PL intensity still remains, which is much more stable (1 or 2 orders of magnitude longer in decay time) than that of irradiated dye-doped PNFs and quantum dots.[11,26] The decay time can be further increased by using pulsed light.

The polarization of the PL emission output from the NF is also investigated. When the polarization orienta-
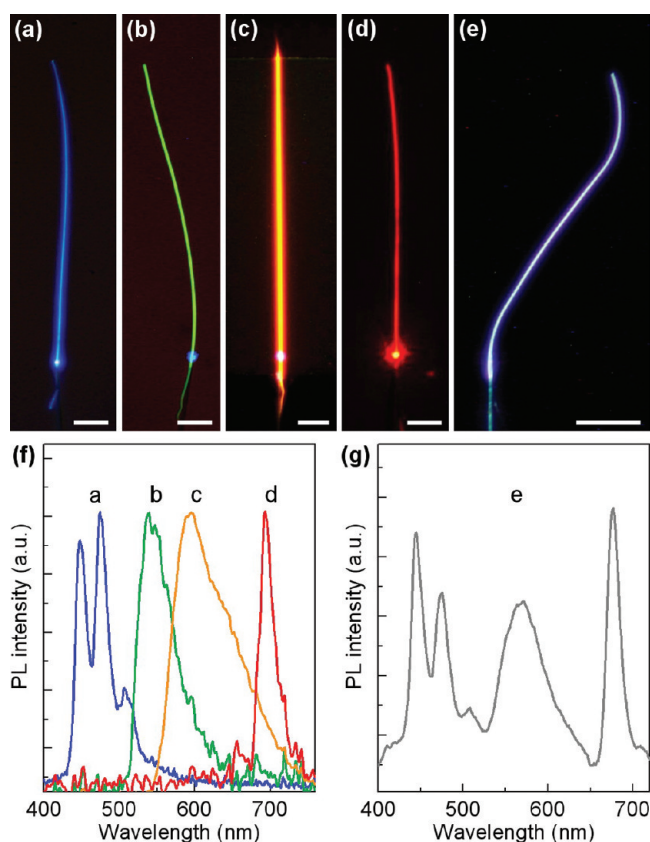
Figure 5. PL microscope images of (a) a 380-nm-diameter perylene-PS NF; (b) a 450-nm-diameter FSS-PAM NF; (c) a 270-nm-diameter Ru(bpy)$_3$Cl$_2$−PAM NF; (d) a 610-nm-diameter ZnPc-PEO NF; and (e) a 430-nm-diameter perylene-RhB-ZnPc-codoped PS NF. In panels a and e λ_{ex} = 355 nm; in panels b and c λ_{ex} = 473 nm; and in panel d λ_{ex} = 650 nm. The PNFs in panels a, b, and d are placed on MgF$_2$ substrate, and in panel c the PNF is suspended across a MgF$_2$ microchannel. Scale bar: (a−e) 50 μm. (f,g) PL spectra corresponding to the doped PNFs shown in panels a−e.

tion of the polarizer is parallel to the dye-doped PNF axis ($P_\parallel$, the output from the PNFs is maximized. Conversely, when the polarization orientation of the polarizer is perpendicular to the PNF axis ($P_\perp$, the output is minimized. Figure 4 shows the microscope images of the output end of a 460-nm-diameter RhB-PS NF taken without (Figure 4a) and with the polarization parallel (Figure 4b) and perpendicular (Figure 4c) to the NF at P_{ex} = 80 nW. The polarization ratio (ρ), defined as ρ = $(P_\parallel - P_\perp)/(P_\parallel + P_\perp)$, is about 0.82. A similar polarization behavior is also observed for the 473-nm excitation light shown in Figure 4 panels d and e with a ρ of ∼0.71. The polarization behavior is not inherited from the excitation light, as there's no obvious difference in the scattered intensity at the input end of the NF (left bright spots in Figure 4d,e).

The polarization behaviors of the RhB-PS NF are mainly caused by the polarization-dependent MgF$_2$-substrate-induced leakage, which is uneven for the two orthogonal polarizations. When the NF is supported by an MgF$_2$ substrate (index of 1.39 vs 1.0 of air), a fraction of evanescent fields[27] will leak into the substrate (refractive index: 1.594 at 570 nm and 1.607 at 473 nm),[28]

in which the fractional leakage is strongly polarization-dependent. As shown in Figure 4f,g, three-dimensional finite-difference time domain (3D-FDTD) simulation[29,30] shows that in the 460-nm-diameter NF, the power (Poynting vector) of the $P_\perp$ modes (λ = 570 nm) suffers higher power leakage than that of the $P_\parallel$ modes, which breaks the balance of the two polarizations at the output, resulting in large polarization ratios of the PL emissions measured at the output of the NF.

The substrate-induced polarization behaviors here depend on the wavelengths of the guided light, the diameters of the NFs, and the difference in the refractive index between the NFs and the substrate.[31,32] Usually, shorter wavelength of the light, larger diameter of the NF, and smaller refractive index of the substrate will result in a lower polarization ratio. For example, with the same 473-nm light, a 580-nm-diameter RhB-PS NF exhibits a much lower polarization ratio (0.1) than that of the 460-nm-diameter RhB-PS NF (0.71), as shown in the Supporting Information (Figure S1).

Benefitted from the enhanced excitation efficiency and photostability of the waveguiding excitation, the waveguiding scheme has readily inspired more opportunities for incorporating a variety of fluorescent dyes into PNFs to generate emissions of desired colors. In Figure 5a−d, we show the optical microscope images of excited PNFs doped with four fluorescent dyes, with PL spectra given in Figure 5f: (a) a 360-nm-diameter PS NF doped with perylene to give a blue color, (b) a 450-nm-diameter polyacrylamide (PAM) NF doped with fluorescein sodium salt (FSS) to give a green color, (c) a 270-nm-diameter PAM NF doped with tris(2,2′-bipyridine)ruthenium(II) chloride [Ru(bpy)$_3$Cl$_2$] to give a orange color, and (d) a 610-nm-diameter PS NF doped with zinc phthalocyanine (ZnPc) to give a red color.

By simultaneously doping multiple fluorescent dyes in a single NF, visually white-light emissions can be obtained. As shown in Figure 5e, when excited by 355-nm light, white-light emission is generated in a 430-nm-diameter perylene-RhB-ZnPc-codoped PS NF. The uniform emission in intensity and color indicates homogeneous distribution of the three dyes along the whole length of the NF. Measured PL spectrum of the perylene-RhB-ZnPc-codoped PS NF is shown in Figure 5g, which covers the whole visible range from 400 to 710 nm. Usually, the emission of the multiple-dye-doped PNF does not exactly accumulate the emission spectra of individual dyes,[12,25] Comparing Figure 5f and Figure 5g, the change of the relative intensities of the 475-nm and 447-nm peaks of perylene indicates the reabsorption of PL of one dye by another. By carefully selecting the dyes to avoid or reduce considerable reabsorption of the PL, as well as controlling their weight ratios in polymer solutions, a visually "white light" emission approximately accumulating the PL of multiple dyes can be obtained. The measured excitation efficiency of the white light emission is about 2% (see Sup-

porting Information, Figure S2), which can be further increased by optimizing the concentrations of the dopants and the wavelength of the excitation light.

In conclusion, we have introduced a waveguiding excitation technique for fluorescent dye-doped single PNFs, which demonstrate a number of advantages including enhanced excitation efficiency, low excitation power operation, tightly confined excitation, and high photostability. Also, waveguiding nanowires or NFs are highly compatible with standard optical fiber systems by means of evanescent coupling, which may offer wider opportunities of the waveguiding-excited NFs in applications such as chemical and biological sensors, multicolor emitting sources, and lasers. In addition, the waveguiding excitation schemes can also be applied to other types of functional light-emitting PNFs, such as conjugated and quantum dot-doped PNFs, suggesting broader perspectives for future nanophotonics.

METHODS

Fabrication of the dye-doped PNFs. The dye-doped PNFs were fabricated by directly drawing from polymer solutions that initially dissolves fluorescent dyes.[18] For example, 250 mg of PS (M_w = 100 000, Alfa Aesar) and 0.3 mg of RhB (Alfa Aesar) were dissolved into 2 g of chloroform, and then the mixture was stirred at room temperature to form a uniform solution. In the drawing process, a tungsten probe with a sharp tip (about several micrometers) fabricated using an electrochemical etching method was used to dip up a small droplet out of the RhB-PS solution onto a glass slide, and then draw a wire out of the droplet quickly. The solvent evaporates instantaneously, leaving a RhB-PS NF on the glass slide. The perylene-PS NFs are drawn from a chloroform solution containing 0.07 wt % perylene (Alfa Aesar) and 5.5 wt % PS. The FSS-PAM NFs are drawn from a water solution containing 0.04 wt % FSS (Alfa Aesar) and 5.5 wt % PAM (M_w = 5 000 000, Aldrich). The Ru(bpy)$_3$Cl$_2$−PAM NFs are drawn from a water solution containing 0.07 wt % Ru(bpy)$_3$Cl$_2$ (Alfa Aesar) and 5.5 wt % PAM. The ZnPc-PS NFs are drawn from a tetrahydrofuran solution containing 0.07 wt % ZnPc (Alfa Aesar) and 5.5 wt % PS. The white-light emitting perylene-RhB-ZnPc-codoped PS NFs are drawn from a chloroform solution containing 0.008 wt % perylene, 0.05 wt % RhB, 0.22 wt % ZnPc, and 20 wt % PS.

Optical Characterization of the Dye-Doped PNFs. As-fabricated PNFs are tailored and manipulated using tungsten probes (driven by three-axis precision stages) under an optical microscope equipped with superlong-working distance objectives. The tungsten probes, with tip sizes less than 100 nm (similar to those used in a scanning tunneling microscope), are fabricated using an electrochemical etching method. The fiber tapers with tip diameters of about 500 nm for coupling light into and out of single PNFs, are taper drawn from a standard optical fiber (SMF-28, Corning). All the excitation sources are continuous-wave monochromatic lasers.

The PL emissions of the PNFs are collected using long working distance microscope objectives and directed to a spectrometer (Maya 2000-Pro, Ocean Optics) and a CCD camera (DXM 1200F, Nikon), respectively. The polarization behaviors of the PL emissions are investigated by placing a linear polarizer between the samples and the detectors (the spectrometer and the CCD). By presetting the orientation of the polarizer parallel or perpendicular to the axis of the PNFs, the polarization-dependent behavior of the output is investigated with high reproducibility.

The optical absorption of the RhB-PS NF in Figure 3c was measured using a broadband light from a fiber-coupled supercontinuum source (SC450, Fianium Ltd.). The absorption A is defined as A = Log (I_0/I_t), where I_t is the transmittance of an RhB doped PS NF, and I_0 is the reference transmittance of an undoped PS NF with the same diameter and length.

Supporting Information Available: Polarization orientation of a 580-nm-diameter RhB-PS NF and measurement of the excita-

tion efficiency of the white-light emission. This material is available free of charge *via* the Internet at http://pubs.acs.org.

REFERENCES AND NOTES

1. Yan, R.; Gargas, D.; Yang, P. Nanowire Photonics. *Nat. Photon* **2009**, *3*, 569–576.
2. Hung, Y.; Duan, X.; Lieber, C. M. Nanowires for Integrated Multicolor Nanophotonics. *Small* **2005**, *1*, 142–147.
3. Mynbaev, D. K.; Scheiner, L. L. *Fiber-Optic Communications Technology*; Prentice Hall: Upper Saddle River, N.J., 2002.
4. Urquhart, P. Review of Rare Earth Doped Fiber Lasers and Amplifiers. *Proc. IEE, Part J* **1988**, *135*, 385–407.
5. Moran-Mirabal, J. M.; Slinker, J. D.; DeFranco, J. A.; Verbridge, S. S.; Ilic, R.; Flores-Torres, S.; Abruna, H.; Malliaras, G. G.; Craighead, H. G. Electrospun Light-Emitting Nanofibers. *Nano Lett.* **2007**, *7*, 458–463.
6. O'Carrol, D.; Lieberwirth, I.; Redmond, G. Melt-Processed Polyfluorene Nanowires as Active Waveguides. *Small* **2007**, *3*, 1178–1183.
7. Benedetto, F. D.; Camposeo, A.; Pagliara, S.; Mele, E.; Persano, L.; Stabile, R.; Cingolani, R.; Pisignano, D. Patterning of Light-Emitting Conjugated Polymer Nanofibres. *Nat. Nanotechnol.* **2008**, *3*, 614–619.
8. Pagliara, S.; Camposeo, A.; Polini, A.; Cingolani, R.; Pisignano, D. Electrospun Light-Emitting Nanofibers as Excitation Source in Microfluidic Devices. *Lab Chip* **2009**, *9*, 2851–2856.
9. Liu, H.; Edel, J. B.; Bellan, L. M.; Craighead, H. G. Electrospun Polymer Nanofibers as Subwavelength Optical Waveguides Incorporating Quantum Dots. *Small* **2006**, *2*, 495–499.
10. Sun, H.; Zhang, H.; Zhang, J.; Wei, H.; Ju, J.; Li, M.; Yang, B. White-Light Emission Nanofibers Obtained from Assembling Aqueous Single-Colored CdTe NCs into a PPV Precursor and PVA Matrix. *J. Mater. Chem.* **2009**, *19*, 6740–6744.
11. Camposeo, A.; Benedetto, F. D.; Stabile, R.; Cingolani, R.; Pisignano, D. Electrospun Dye-Doped Polymer Nanofibers Emitting in the Near Infrared. *Appl. Phys. Lett.* **2007**, *90*, 143115.
12. Vohra, V.; Calzaferri, G.; Destri, S.; Pasini, M.; Porzio, W.; Botta, C. Toward White Light Emission through Efficient Two-Step Energy Transfer in Hybrid Nanofibers. *ACS Nano* **2010**, *4*, 1409–1416.
13. O'Carroll, D.; Lieberwirth, I.; Redmond, G. Microcavity Effects and Optically Pumped Lasing in Single Conjugated Polymer Nanowires. *Nat. Nanotechnol.* **2007**, *2*, 180–184.
14. Zhao, Y. S.; Peng, A.; Fu, H.; Ma, Y.; Yao, J. Nanowire Waveguides and Ultraviolet Lasers Based on Small Organic Molecules. *Adv. Mater.* **2008**, *20*, 1661–1665.
15. Camposeo, A.; Benedetto, F. D.; Stabile, R.; Neves, A. A. R.; Cingolani, R.; Pisignano, D. Laser Emission from Electrospun Polymer Nanofibers. *Small* **2009**, *5*, 562–566.
16. Ma, H.; Jen, A. K.-Y.; Dalton, L. R. Polymer-Based Optical Waveguides: Materials, Processing, and Devices. *Adv. Mater.* **2002**, *14*, 1339–1365.

17. Law, M.; Sirbuly, D. J.; Johnson, J. C.; Goldberger, J.; Saykally, R. J.; Yang, P. D. Nanoribbon Waveguides for Subwavelength Photonics Integration. *Science* **2004**, *305*, 1269–1273.

18. Sirbuly, D. J.; Tao, A.; Law, M.; Fan, R.; Yang, P. Multifunctional Nanowire Evanescent Wave Optical Sensors. *Adv*. *Mater* **2007**, *19*, 61–66.

19. Yang, Q.; Jiang, X.; Guo, X.; Chen, Y.; Tong, L. Hybrid Structure Laser based on Semiconductor Nanowires and a Silica Microfiber Knot Cavity. *Appl. Phys. Lett.* **2009**, *94*, 101108.

20. Tong, L.; Gattass, R. R.; Ashcom, J. B.; He, S. L.; Lou, J. Y.; Shen, M. Y.; Maxwell, I.; Mazur, E. Subwavelength-Diameter Silica Wires for Low-Loss Optical Wave Guiding. *Nature* **2003**, *426*, 816–819.

21. Gu, F.; Zhang, L.; Yin, X.; Tong, L. Polymer Single-Nanowire Optical Sensors. *Nano Lett.* **2008**, *8*, 2757–2761.

22. Gu, F.; Yin, X.; Yu, H.; Wang, P.; Tong, L. PANI-PS Single-Nanowire Devices for Highly Selective Optical Detection of Gas Mixtures. *Opt. Express* **2009**, *17*, 11230–11235.

23. Huang, Z. M.; Zhang, Y. Z.; Kotaki, M.; Ramakrishna, S. A Review on Polymer Nanofibers by Electrospinning and Their Applications in Nanocomposites. *Compos. Sci. Technol.* **2003**, *63*, 2223–2253.

24. Huang, K.; Yang, S.; Tong, L. Modeling of Evanescent Coupling Between Two Parallel Optical Nanowires. *Appl. Opt.* **2007**, *46*, 1429–1434.

25. Lakowicz, J. R. *Principles of Fluorescence Spectroscopy;* 3rd ed., Springer-Verlag: Berlin, Heidelberg, 2006.

26. van Sark, W. G. J. H. M.; Frederix, P. L. T. M.; Bol, A. A.; Gerritsen, H. C.; Meijerink, A. Blueing, Bleaching, and Blinking of Single CdSe ZnS Quantum Dots. *Chemphyschem* **2002**, *3*, 871–879.

27. Tong, L.; Lou, J.; Mazur, E. Single-Mode Guiding Properties of Subwavelength-Diameter Silica and Silicon Wire Waveguides. *Opt. Express* **2004**, *12*, 1025–1035.

28. Kasarova, S. N.; Sultanova, N. G.; Ivanov, C. D.; Nikolov, I. V. Analysis of the Dispersion of Optical Plastic Materials. *Opt. Mater.* **2007**, *29*, 1481–1490.

29. Taflove, A.; Hagness, S. C. *Computational Electrodynamics: The Finite-Difference Time-Domain Method;* 3rd ed., Artech House Antennas and Propagation Library: Boston, MA, 2005.

30. Kawano, K.; Kitoh, T. *Introduction to Optical Waveguide Analysis: Solving Maxwell's Equations and the Schrödinger Equation*. Wiley-Interscience: New York, 2001.

31. Giblin, J.; Protasenko, V.; Kuno, M. Wavelength Sensitivity of Single Nanowire Excitation Polarization Anisotropies Explained through a Generalized Treatment of Their Linear Absorption. *ACS Nano* **2009**, *3*, 1979–1987.

32. Dong, G.; Xiao, X.; Chi, Y.; Qian, B.; Liu, X.; Ma, Z.; Wu, E.; Zeng, H.; Chen, D.; Qiu, J. Size-Dependent Polarized Photoluminescence from $Y_3Al_5O_{12}$ Eu^{3+} Single Crystalline Nanofiber Prepared by Electrospinning. *J. Mater. Chem.* **2010**, *20*, 1587–1593.